Modern Physics Letters A

MADANALYSIS 5 Implementation of the W' Search in Events with a Charged Lepton and Missing Transverse Momentum at $\sqrt{s} = 13\,\text{TeV}$ and 139 fb^{-1} Luminosity with the ATLAS detector

Kyungmin Park[a], Ui Min[b], SooJin Lee[c], Won Jun[d]

University of Seoul, Republic of Korea[a]
KAIST, Republic of Korea[b]
Konkuk University Seoul, Republic of Korea[c]
Seoul National University, Republic of Korea[d]

We present the MadAnalysis 5 implementation of the heavy charged gauge boson search to recast the analysis of its decay into one charged lepton and missing transverse momentum. Signal events describing $pp \to W' \to l\,\nu_l$ ($l = e$ or μ) at $\sqrt{s} = 13\,\text{TeV}$ in the sequential standard model are generated by the MadGraph5_aMC@NLO at leading order. The corresponding signal cross-sections for both electron and muon channels vary from 195 fb to 0.238 fb depending on the pole mass of the W' boson in the range of 2 TeV to 6 TeV. We validate our implementation by comparing the transverse mass distributions of our signal prediction to those of the ATLAS analysis for an integrated luminosity of $139\,\text{fb}^{-1}$.

Keywords: gauge theory, extended gauge sector, extra gauge boson search.

1. Introduction

One of the testable models at the LHC is the Sequential Standard Model (SSM), where new heavy gauge bosons W' and Z' couple to the SM fermions with the same strength as the SM weak gauge bosons [1,2]. In a simplified model approach, the SSM extends the SM gauge sector by an additional $SU(2)'$ symmetry, $SU(3)_c \times SU(2)_L \times U(1) \times SU(2)'$. Here, the new gauge bosons get their heavy masses after spontaneous symmetry breaking at the energy scale that is higher than the electroweak scale. We assume that any detail on the extended gauge symmetry breaking mechanism can be factored out and ignored at the LHC scale. For simplicity, we ignore interactions including Z' and only consider those between W' and the left-handed SM fermions. Its triple gauge couplings and couplings to Higgs are also neglected.

Under the MadAnalysis 5 [3–6] framework, we reimplement the ATLAS-EXOT-2018-30 analysis [7], a search for a W' signal at the LHC using the ATLAS detector and $139\,\text{fb}^{-1}$ of proton-proton collisions, in the $p\,p \to W' \to l\,\nu_l$ ($l = e, \mu$) channel, as shown in Fig. 1. We then validate the reimplementation by comparing our signal predictions to those from the official ATLAS results, with W' masses varying from 2 TeV to 6 TeV.

In section 2, we define the objects such as electron, muon, jet and missing trans-

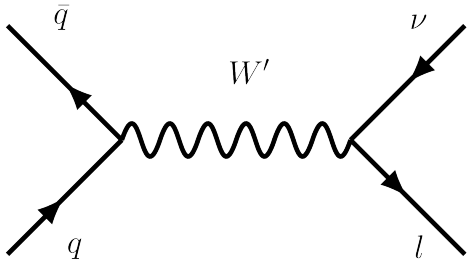

Fig. 1. W' boson contribution to the production of a lepton and a neutrino in $q\bar{q}$ scattering.

verse energy, and we present how to select events for the electron and muon channels. In section 3, we describe processes of event generation for the decay channels $p\,p \to W' \to l\,\nu_l$ ($l = e, \mu$) and compare the results with those of ATLAS analysis. We summarise our work in section 4.

2. Description of the analysis

The analysis targets a signature in which a heavy W' boson decays into a single lepton and a neutrino. To extract the heavy charged gauge boson signal, events including high missing transverse energy ($\not{E}_T$) and a charged lepton with high transverse momentum (p_T) are selected.

2.1. *Object definitions*

As our main targets are the electron channel ($p\,p \to W' \to e\,\nu$) and the muon channel ($p\,p \to W' \to \mu\,\nu$), the analysis requires the reconstruction and identification of electrons and muons with high p_T, following the object selections defined in the considered ATLAS study [7].

For the electron candidates, they must have a transverse energy $E_T > 65\,\text{GeV}$ and a pseudo-rapidity $|\eta| < 2.47$, where the barrel-endcap transition region $1.37 < |\eta| < 1.52$ is excluded. The candidates are required to satisfy the following isolation criteria based on both calorimeter and tracking measurements: $E_T^{cone20}/p_T < 0.06$ for calorimeter isolation and $p_T^{cone20}/p_T < 0.06$ for track isolation. Here, p_T^{cone20} $\left(E_T^{cone20}\right)$ is computed by summing the transverse momentum (energy) of all tracks (energy deposits) within a cone centered around the electron track, with a cone size of $\Delta R = 0.2$ [8]. The reconstruction and identification efficiencies and the resolution of electrons are implemented in the DELPHES 3 [9] card following Refs. [7,8]. In the $p_T > 50\,\text{GeV}$ region, for example, this yields an electron reconstruction efficiency of 81.7%.

For the muon candidates, we require high-p_T muons with $p_T > 55\,\text{GeV}$ and $0.1 < |\eta| < 2.4$. Those with pseudo-rapidity in the range of $1.01 < |\eta| < 1.1$ are vetoed due to the significant drop in the efficiencies [10]. The candidates must

Table 1. Object selections

Object	$E_T^e(p_T^{\mu,jet})$	$\lvert\eta\rvert$	Identification
e	> 65 GeV	< 1.37, $[1.52, 2.47]$	tight identification
μ	> 55 GeV	$[0.1, 1.01]$, $[1.1, 2.4]$	high-p_T identification
jet	> 20 GeV	< 2.4	-
	> 30 GeV	$[2.4, 2.5]$	-

Table 2. Isolation criteria

Object	Calorimeter isolation	Track isolation	ΔR
e	$E_T^{cone20}/p_T < 0.06$	$p_T^{cone20}/p_T < 0.06$	0.2
μ	-	$p_T^{cone30}/p_T < 0.15$	$\min(10\,GeV/p_T, 0.3)$ for $p_T > 1\,GeV$

pass track-based isolation criteria, $p_T^{cone30}/p_T < 0.15$ where p_T^{cone30} is defined as the scalar sum of the transverse momenta of all tracks with $p_T > 1\,\text{GeV}$ in a cone size of $\Delta R = \min(10\,\text{GeV}/p_T, 0.3)$ around the muon transverse momentum p_T, excluding the muon track itself [10]. The reconstruction and identification efficiencies and resolution of muons are implemented in the Delphes card following Refs. [7, 10]. For instance, this gives a muon efficiency of 53% for $p_T > 3\,\text{TeV}$.

For the jet candidates, jet-reconstruction is achieved with the anti-k_T algorithm [11] as implemented in FastJet [12,13] with a jet radius parameter $\Delta R = 0.4$. The kinematical region of interest is chosen by defining the jet candidates as those satisfying $p_T > 20\,\text{GeV}$ for $|\eta| < 2.4$ and $p_T > 30\,\text{GeV}$ for $2.4 < |\eta| < 2.5$. We enforce an overlap removal procedure with the electron collection, removing jets lying within a cone of $\Delta R(j, e) = 0.1$ of an electron.

The missing transverse energy $\not{E}_T$ is evaluated by the vector sum of the transverse momenta of the following components: leptons, photons[a], and jets. Table 1 and Table 2 show the summary for these object selections and isolation criteria, respectively.

2.2. *Event selection*

The missing transverse energy ($\not{E}_T$) and the transverse mass (m_T) observables are used to select events from the electron and muon channels. Here, $m_T(l, \not{E}_T)$ can be calculated by following formula,

$$m_T(l, \not{E}_T) = \sqrt{2\, p_T^l \not{E}_T\, (1 - \cos\phi_{l\nu})}\ , \tag{1}$$

where p_T^l is the lepton transverse momentum, and $\phi_{l\nu}$ refers the azimuthal angle difference between the lepton and missing energy momenta.

For the electron channel, each event must have exactly one electron satisfying the conditions stated in Section 2.1. Any events containing additional electrons or muons

[a]Photons are reconstructed as defined in the default ATLAS parameterization in Delphes 3 [9].

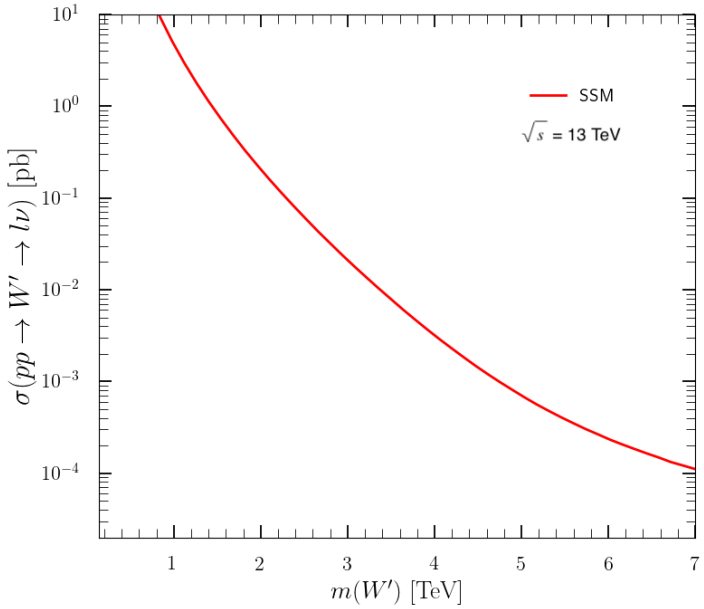

Fig. 2. Cross-sections for W' production and its decay into one lepton-neutrino pair, at leading order and at $\sqrt{s} = 13\,\text{TeV}$ as a function of W' mass.

with $p_T > 20\,\text{GeV}$ are vetoed. Events are then required to satisfy $\not{E}_T > 65\,\text{GeV}$ and $m_T(e, \not{E}_T) > 130\,\text{GeV}$.

For the muon channel, there must be exactly one muon passing the selections listed in Section 2.1. Events are vetoed if they feature electrons that satisfy both $p_T > 20\,\text{GeV}$ and $\Delta R(e, \mu) > 0.1$. Events including any additional muons with $p_T > 20\,\text{GeV}$ are also vetoed. The missing transverse energy and the transverse mass must satisfy $\not{E}_T > 55\,\text{GeV}$ and $m_T(\mu, \not{E}_T) > 110\,\text{GeV}$.

3. Validation

3.1. *Event generation*

The SSM with heavy gauge bosons has been implemented in the FeynRules package[b] [14], from which UFO model files have been generated. They are then imported into MadGraph5_aMC@NLO [15] to generate the signal samples relevant for the validation of our re-implementation. In the SSM simplified model set-up, we switch off all W' couplings to right-handed SM fermions ($\kappa_R = 0$ in the model conventions), and set the couplings to the left-handed SM fermions to be the same as those of the

[b]See the webpage http://feynrules.irmp.ucl.ac.be/wiki/Wprime.

SM W boson ($\kappa_L = 1$ in the model conventions). The decay width of the W' boson is finally automatically determined by its mass and couplings to fermions within MadGraph5_aMC@NLO by means of MadSpin [16] and MadWidth [17].

Signal events describing the $pp \to W' \to l\,\nu_l$ ($l = e, \mu$) process are generated[c]. Both on-shell and off-shell heavy gauge boson contributions are included. The interference between the SM contributions and the SSM ones is, however, not considered, since the SM W bosons are mostly produced almost on-shell and the mass gap between the W and W' bosons is much larger than their decay widths. Signal events with various W' masses are generated by MadGraph5_aMC@NLO v2.6.7 [15] at leading order (LO), with the LO set of NNPDF 2.3 parton densities with $\alpha_s(m_Z) = 0.130$ [18], as obtained from LHAPDF6 [19]. We use Pythia 8.224 [20] for parton showering and hadronisation.

The following commands were used to generate events in MadGraph5_aMC @NLO.

```
import model WEff_UFO
define p = g u c d s u~ c~ d~ s~
define l+ = e+ mu+
define l- = e- mu-
define vl = ve vm vt
define vl~ = ve~ vm~ vt~
generate p p > wp- > l- vl~
add process p p > wp+ > l+ vl
output
```
(2)

In the `param_card` file, `kr` and `kl` are set to 0 and 1 respectively, and the W' mass `MWP` varies from 2 TeV to 6 TeV with its decay width being automatically calculated. In the `run_card` file, both `fixed_ren_scale` and `fixed_fac_scale` are set to `False`, and thus the QCD renormalization and collinear factorization scales are set to the averaged transverse mass of the final state particles. Half a million signal events are generated for each mass point. The corresponding cross-sections estimated by MadGraph5_aMC@NLO for various W' masses are shown in Fig. 2. For a mass of 2(6) TeV for example, we obtain the cross-sections of 195(0.238) fb. Overall, the cross-sections are in agreement with those from Fig. 2 in the considered ATLAS paper [7].

3.2. *Comparison with ATLAS result for a luminosity of* $139\,\mathrm{fb}^{-1}$

In the absence of any official ATLAS cutflow in Ref. [7], we decided to validate our implementation by comparing the m_T-distributions of our W' signal events after

[c]Events with hadronic taus in the final state are not generated.

Table 3. Comparison of MadAnalysis 5 and ATLAS predictions for the m_T-spectrum in the electron channel ($W' \to e\,\nu$). The overflow bins are not accounted for. The relative differences (δ) between our ratios (R^{MA5}) and those of ATLAS (R^{ATLAS}) are calculated by eq. (3).

W' mass	m_T range(GeV)	130 − 400	400 − 600	600 − 1000	1000 − 2000	2000 − 3000	3000 − 10000
2 TeV	R^{ATLAS}	0.0341 ± 0.0019	0.0428 ± 0.0029	0.130 ± 0.009	0.725 ± 0.046	0.0672 ± 0.0175	0.000190 ± 0.000017
	R^{MA5}	0.0329	0.0429	0.134	0.726	0.0644	0.000173
	difference(%)	3.50	0.148	2.75	0.0468	4.12	9.25
3 TeV	R^{ATLAS}	0.0415 ± 0.0017	0.0355 ± 0.0019	0.0770 ± 0.0049	0.272 ± 0.016	0.522 ± 0.029	0.0528 ± 0.0140
	R^{MA5}	0.0409	0.0345	0.0779	0.273	0.521	0.0530
	difference(%)	1.50	2.86	1.15	0.423	0.114	0.377
4 TeV	R^{ATLAS}	0.0836 ± 0.0028	0.0563 ± 0.0025	0.0943 ± 0.0052	0.189 ± 0.010	0.210 ± 0.011	0.367 ± 0.019
	R^{MA5}	0.0812	0.0566	0.0875	0.182	0.212	0.381
	difference(%)	2.86	0.503	7.24	3.46	0.786	3.77
5 TeV	R^{ATLAS}	0.159 ± 0.005	0.101 ± 0.004	0.147 ± 0.008	0.200 ± 0.011	0.118 ± 0.006	0.275 ± 0.015
	R^{MA5}	0.159	0.0955	0.136	0.185	0.119	0.306
	difference(%)	0.0985	5.44	7.69	7.63	1.25	11.1
6TeV	R^{ATLAS}	0.226 ± 0.007	0.141 ± 0.005	0.197 ± 0.010	0.230 ± 0.012	0.0848 ± 0.0045	0.121 ± 0.006
	R^{MA5}	0.230	0.135	0.186	0.213	0.0844	0.151
	difference(%)	1.76	4.26	5.55	7.22	0.464	24.8

Table 4. Same as in Table 3, but for the muon channel ($W' \to \mu\,\nu$)

W'mass	m_T range(GeV)	110 − 400	400 − 600	600 − 1000	1000 − 2000	2000 − 3000	3000 − 10000
2 TeV	R^{ATLAS}	0.0443 ± 0.0026	0.0537 ± 0.0036	0.152 ± 0.011	0.606 ± 0.054	0.138 ± 0.020	0.00633 ± 0.00453
	R^{MA5}	0.0416	0.0547	0.165	0.608	0.128	0.00368
	difference(%)	6.21	1.81	8.47	0.246	7.23	41.9
3 TeV	R^{ATLAS}	0.0544 ± 0.0039	0.0426 ± 0.0033	0.0955 ± 0.0085	0.302 ± 0.035	0.356 ± 0.053	0.150 ± 0.039
	R^{MA5}	0.0491	0.0427	0.104	0.348	0.328	0.128
	difference(%)	9.84	0.112	9.05	15.3	7.745	14.6
4 TeV	R^{ATLAS}	0.107 ± 0.010	0.0634 ± 0.0064	0.105 ± 0.011	0.212 ± 0.030	0.224 ± 0.039	0.289 ± 0.090
	R^{MA5}	0.0994	0.0610	0.109	0.240	0.241	0.250
	difference(%)	7.21	3.73	3.83	13.2	7.78	13.6
5 TeV	R^{ATLAS}	0.198 ± 0.015	0.108 ± 0.009	0.152 ± 0.013	0.204 ± 0.023	0.119 ± 0.020	0.219 ± 0.072
	R^{MA5}	0.184	0.103	0.150	0.210	0.140	0.212
	difference(%)	6.86	4.45	1.21	3.01	18.1	3.38
6 TeV	R^{ATLAS}	0.272 ± 0.012	0.146 ± 0.008	0.194 ± 0.011	0.215 ± 0.017	0.0771 ± 0.0109	0.0954 ± 0.309
	R^{MA5}	0.262	0.145	0.194	0.217	0.0803	0.103
	difference(%)	3.67	1.15	0.419	1.02	4.14	7.43

all cuts with those of ATLAS. Here, m_T refers to the transverse mass of the system comprising the signal lepton and the missing momentum.

In Table 3 (Table 4), we present the comparison of m_T-distributions for m_T values ranging from 130 (110) GeV to 10 TeV in the electron (muon) channel between our MadAnalysis 5 (MA5) results and the ATLAS official results. For each W' mass, there are six signal regions defined according to their m_T ranges. We define

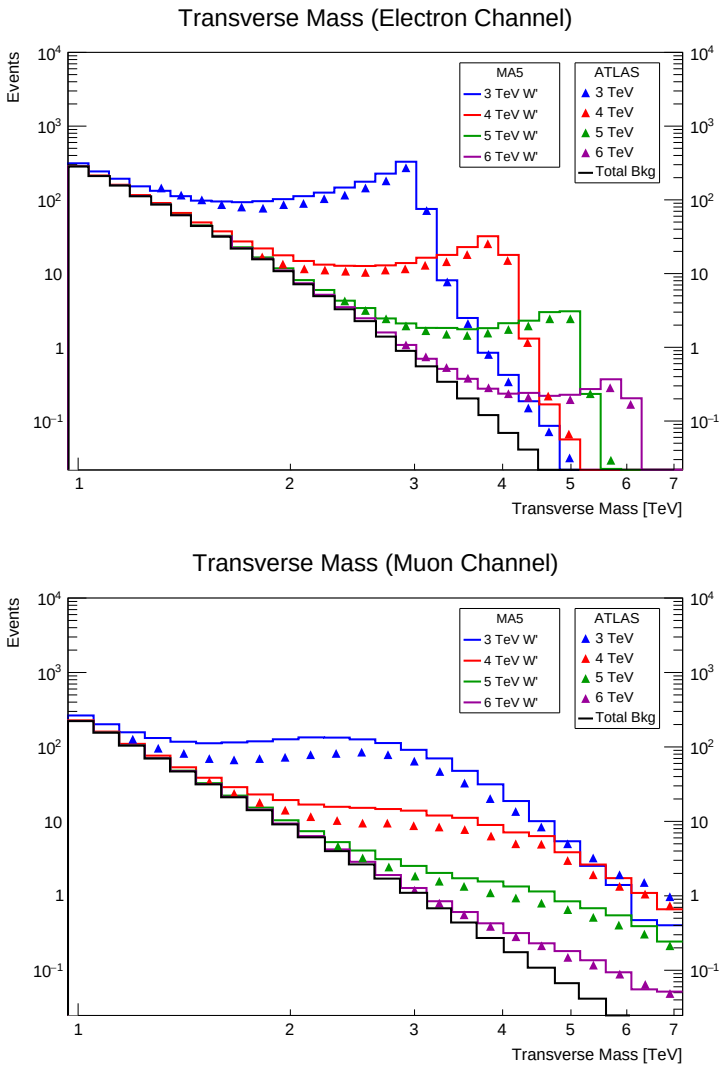

Fig. 3. m_T-distributions in the electron channel and muon channel. The solid lines represent our signal predictions for each W' mass in MA5, and the triangle dots represent those of ATLAS.

the relative differences (δ) between MA5 predictions and ATLAS official estimates as below,

$$\delta = \frac{\left|R^{ATLAS} - R^{MA5}\right|}{R^{ATLAS}} \times 100[\%] \tag{3}$$

where R^{MA5} and R^{ATLAS} refer to the ratio of the number of events in each region over the total number of events for each W' mass, for our analysis and for ATLAS study respectively. The relative differences (δ) are up to 20% or within the

uncertainty range given by ATLAS in most signal regions. In the electron channel, the differences are all below 10% except for 24.8% for the [3, 10] TeV bin. In the muon channel, for regions of m_T below 1 TeV, the differences are all under 10%, while some differences reach up to around 15% for those over 1 TeV. There is one m_T-region whose relative difference far exceeds 20% — when the transverse mass lies in the $[3, 10]$ TeV window for scenarios in which 2 TeV W' boson decays into a muon-neutrino pair. However, this huge discrepancy can be well resolved when considering the large uncertainty associated with this region that is reported by the ATLAS collaboration. Therefore, we confirm that our reimplementation predictions are in good agreement with the official ATLAS results.

Fig. 3 shows the transverse mass distributions with W' masses varying from 3 TeV to 6 TeV. The signal predictions of our MadAnalysis 5 implementation as well as those from ATLAS are stacked on top of the total background extracted from the official ATLAS results [7]. In both the electron and muon channels, we obtain a good agreement between the figures of our reimplementation and the original analysis [7].

4. Conclusions

We have presented the reimplementation of the heavy charged gauge boson search ATLAS-EXOT-2018-30 [7] in the MadAnalysis 5 framework. Samples of signal events describing the $pp \to W' \to l\,\nu_l$ ($l = e$ or μ) process at $\sqrt{s} = 13\,\text{TeV}$ in the sequential standard model have been generated with MadGraph5_aMC@NLO at LO, and the simulation of the ATLAS detector has been achieved with Delphes 3. We have compared predictions made by MadAnalysis 5 with the results provided by the ATLAS collaboration. We have considered various benchmark scenarios in both the electron and the muon channel, where a good agreement at the level of m_T spectra is achieved between our reinterpretation and ATLAS results. Relative differences of at most 20% have been observed, with the most extreme discrepancy being well explained by the large uncertainty populating the corresponding signal region.

The material that has been used for the validation of this implementation is available, together with the MadAnalysis 5 C++ code, at the MA5 dataverse (https://doi.org/10.14428/DVN/GLWLTF) [21].

Acknowledgments

We are very grateful to the ATLAS EXOT conveners for their help and all the additional information they provided, and to Magnar Bugge in particular who were invaluable in our validation process. We would also like to express our sincere gratitude to all the tutors at the second MadAnalysis 5 workshop on LHC recasting.

References

1. G. Altarelli, B. Mele and M. Ruiz-Altaba, *Z. Phys. C* **45**, 109 (1989), [Erratum: Z.Phys.C 47, 676 (1990)].
2. B. Fuks and R. Ruiz, *JHEP* **05**, 032 (2017), arXiv:1701.05263 [hep-ph].
3. E. Conte, B. Fuks and G. Serret, *Comput. Phys. Commun.* **184**, 222 (2013), arXiv:1206.1599 [hep-ph].
4. E. Conte, B. Dumont, B. Fuks and C. Wymant, *Eur. Phys. J. C* **74**, 3103 (2014), arXiv:1405.3982 [hep-ph].
5. B. Dumont, B. Fuks, S. Kraml, S. Bein, G. Chalons, E. Conte, S. Kulkarni, D. Sengupta and C. Wymant, *Eur. Phys. J. C* **75**, 56 (2015), arXiv:1407.3278 [hep-ph].
6. E. Conte and B. Fuks, *Int. J. Mod. Phys. A* **33**, 1830027 (2018), arXiv:1808.00480 [hep-ph].
7. ATLAS Collaboration, G. Aad *et al.*, *Phys. Rev. D* **100**, 052013 (2019), arXiv:1906.05609 [hep-ex].
8. ATLAS Collaboration, G. Aad *et al.*, *JINST* **14**, P12006 (2019), arXiv:1908.00005 [hep-ex].
9. DELPHES 3 Collaboration, J. de Favereau, C. Delaere, P. Demin, A. Giammanco, V. Lemaître, A. Mertens and M. Selvaggi, *JHEP* **02**, 057 (2014), arXiv:1307.6346 [hep-ex].
10. ATLAS Collaboration, G. Aad *et al.*, *Eur. Phys. J. C* **76**, 292 (2016), arXiv:1603.05598 [hep-ex].
11. M. Cacciari, G. P. Salam and G. Soyez, *JHEP* **04**, 063 (2008), arXiv:0802.1189 [hep-ph].
12. M. Cacciari, G. P. Salam and G. Soyez, *Eur. Phys. J. C* **72**, 1896 (2012), arXiv:1111.6097 [hep-ph].
13. M. Cacciari and G. P. Salam, *Phys. Lett. B* **641**, 57 (2006), arXiv:hep-ph/0512210.
14. A. Alloul, N. D. Christensen, C. Degrande, C. Duhr and B. Fuks, *Comput. Phys. Commun.* **185**, 2250 (2014), arXiv:1310.1921 [hep-ph].
15. J. Alwall, R. Frederix, S. Frixione, V. Hirschi, F. Maltoni, O. Mattelaer, H. S. Shao, T. Stelzer, P. Torrielli and M. Zaro, *JHEP* **07**, 079 (2014), arXiv:1405.0301 [hep-ph].
16. P. Artoisenet, R. Frederix, O. Mattelaer and R. Rietkerk, *JHEP* **03**, 015 (2013), arXiv:1212.3460 [hep-ph].
17. J. Alwall, C. Duhr, B. Fuks, O. Mattelaer, D. G. Öztürk and C.-H. Shen, *Comput. Phys. Commun.* **197**, 312 (2015), arXiv:1402.1178 [hep-ph].
18. R. D. Ball *et al.*, *Nucl. Phys. B* **867**, 244 (2013), arXiv:1207.1303 [hep-ph].
19. A. Buckley, J. Ferrando, S. Lloyd, K. Nordström, B. Page, M. Rüfenacht, M. Schönherr and G. Watt, *Eur. Phys. J. C* **75**, 132 (2015), arXiv:1412.7420 [hep-ph].
20. T. Sjöstrand, S. Ask, J. R. Christiansen, R. Corke, N. Desai, P. Ilten, S. Mrenna, S. Prestel, C. O. Rasmussen and P. Z. Skands, *Comput. Phys. Commun.* **191**, 159 (2015), arXiv:1410.3012 [hep-ph].
21. K. Park, S. Lee, W. Jun and U. Min, *https://doi.org/10.14428/DVN/GLWLTF* (2020).